Global NEST Journal, Vol 25, No 2, pp 36-43

Synthesis of $Fe_3O_4/SiO_2/NiO$ magnetic composite: Evaluation of its catalytic activity for methylene blue degradation

Hariani P.L.[1*], Said M.[1], Salni[2], Rachmat A.[1], Aprianti N.[3], and Sthephanie E.A.[1]
[1]Department of Chemistry, Faculty of Mathematics and Natural Sciences, Universitas Sriwijaya, Ogan Ilir, Indonesia
[2]Department of Biology, Faculty of Mathematics and Natural Sciences, Universitas Sriwijaya, Ogan Ilir, Indonesia
[3]Chemical Engineering Department, Faculty of Engineering, Universitas Sriwijaya, Ogan Ilir, Indonesia
Received: 20/07/2022, Accepted: 27/11/2022, Available online: 28/11/2022
*to whom all correspondence should be addressed: e-mail: puji_lukitowati@mipa.unsri.ac.id
https://doi.org/10.30955/gnj.004407

Graphical abstract

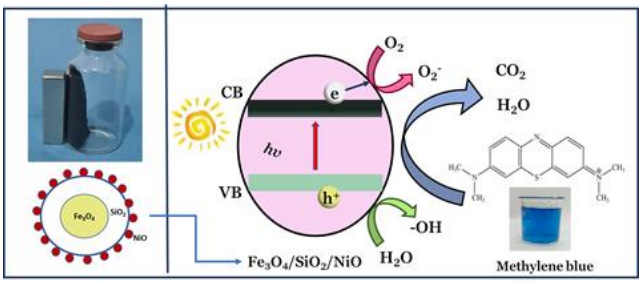

Abstract

Photocatalytic degradation for wastewater treatment is a method that has recently attracted attention. In this research, a synthesized composite of $Fe_3O_4/SiO_2/NiO$ with magnetic properties was used for the photocatalytic degradation of methylene blue dye under UV light. Furthermore, the composites were characterized using XRD, FTIR, BET surface area, SEM-EDS, VSM, and UV-DRS. The results showed that the $Fe_3O_4/SiO_2/NiO$ composite is magnetic with a saturation magnetization of 53.84 emu/g. The $Fe_3O_4/SiO_2/NiO$ composite has a surface area of 128.8 m^2/g, large than Fe_3O_4 and Fe_3O/SiO_2. The $Fe_3O_4/SiO_2/NiO$ composite has a band gap of 2.83 eV. The photocatalytic activity of $Fe_3O_4/SiO_2/NiO$ composite against the methylene blue dye exhibited high degradation efficiency reaching 98.51 %. The pseudo-first-order is appropriate to describe the kinetics model of photocatalytic degradation on methylene blue dye . The decrease in the degradation efficiency of the $Fe_3O_4/SiO_2/NiO$ composite after 5 times for the photocatalytic degradation of methylene blue dye from 98.02 % to 94.97 % indicates that the catalyst has high stability. Considering these results, the $Fe_3O_4/SiO_2/NiO$ composites could be used as a potential catalyst in industrial wastewater.

Keywords: $Fe_3O_4/SiO_2/NiO$, magnetic composite, photocatalytic, degradation, methylene blue dye

1. Introduction

Wastewater discharged from industry often contains pathogenic organisms in organic and inorganic contaminants that harm the environment (Pham *et al.,* 2018). It contains dyes with several characteristics, including a large volume of waste, high chromaticity, high organic matter concentration, poor biodegradability, disturbing aesthetics, and blocking the transmission of sunlight, thereby reducing the photosynthetic activity in the waters. Additionally, a low concentration of dye (< 1 mg/L) can disturb the waters (Vandevivere *et al.,* 1998). Methylene blue ($C_{16}H_{18}ClN_3S$) is a cationic dye widely used in the coloring industry and as a chemical indicator (Khodai *et al.,* 2013; Kuang *et al.,* 2020). It has an aromatic group and a complex structure that is hydrophilic and stable to light, temperature, and chemicals (Hou *et al.,* 2018).

Various technologies, such as biological, physical, and chemical treatment have been used to reduce the concentration of dyes. The methods used to removal dye include adsorption (Ziaadini *et al.,* 2019), precipitation (Ali *et al.,* 2006), coagulation-flocculation (Moghaddam *et al.,* 2010), filtration (David *et al.,* 2020), ozonation (Dias *et al.,* 2019) and others. Adsorption is often applied because it effectively reduces the concentration of dyes but causes secondary pollutants (Fu *et al.,* 2019). Presently, Advanced Oxidation Processes (AOPs) have been an effective method for degrading organic pollutants (Behzadi *et al*., 2020) due to their low cost and high efficiency (Behzadi *et al*., 2020; Jarariya, 2022).

The AOPs method often used is heterogeneous photocatalysis based on semiconductor materials. The irradiation of the semiconductor by photons on the band gap energy produces positive and negative electrons. Furthermore, the positive hole reacts with a water molecule to produce a hydroxyl radical (•OH), while electrons react with O_2 molecules to form superoxide radicals ($•O_2$). The hydroxyl and superoxide radicals degrade dye into smaller non-toxic compounds, CO_2 and H_2O (Gao *et al.,* 2013; Salomon *et al.,* 2012). The several semiconductor materials used include TiO_2 (Hou *et al.,* 2018), $NiFe_2O_4$ (Hariani *et al.,* 2021), NiO (Lett *et al.,* 2022), ZnO (Chen *et al.,* 2017), and $CoFe_2O_4$ (Loan *et al.,* 2019).

Nickel oxide (NiO) is a p-type transition metal oxide semiconductor with a band gap of about 3.5 eV, antiferromagnetic, high conductivity, stable, and catalytic properties (Hosny, 2011; D'Amario *et al.,* 2018; Barakat *et al.,* 2013). It performs effectively in the photodegradation of orange II dye (Khan *et al.,* 2022), methylene blue (Let *et al.,* 2022; Wan *et al.,* 2013), and methyl orange dye (Barzinjy *et al.,* 2020). The combination of magnetic ferrite with NiO is a strategy to increase the efficiency of the catalytic process and the separation of the catalyst from the solution. The magnetic ferrite serves as a core. SiO_2 is a layer to avoid the interaction between NiO and magnetic ferrite. The core-shell-shell structure increases the surface area, reduces the cost of catalyst usage, and increases lifespan (Channei *et al.,* 2014; Girginova *et al.,* 2010). For example, Fe_3O_4 coated with activated carbon and TiO_2 showed better catalytic ability than used with only TiO_2 (Gebrezgiabher *et al.,* 2019).

This research synthesized a magnetic composite of Fe_3O_4/SiO_2/NiO, with Fe_3O_4 as the core, SiO_2 as the inner shell, and NiO as the outer shell. Fe_3O_4 is the most widely used magnetic iron oxide compared to other ferrite compounds with an inverse spinel structure and superparamagnetic. The advantage of using Fe_3O_4 as a core in composites, after being used for photocatalytic degradation process, the composite can easily be separated from the solution using an external magnet, without filtering. Fe_3O_4/SiO_2/NiO were applied for photocatalytic degradation of methylene blue dye under UV light irradiation. Finally, the kinetic photocatalytic degradation and reusability of these composites were investigated.

2. Materials and methods

2.1. Materials

The materials used are of analytical grade without purification, including $FeCl_2{\cdot}4H_2O$, $FeCl_3{\cdot}6H_2O$, $FeCl_3{\cdot}6H_2O$, $NiCl_2{\cdot}6H_2O$, NaOH, HCl, C_2H_5OH, NH_4OH, NH_4HCO_3, Tetraethyl orthosilicate (TEOS), Diethylene Glycol (DEG), methylene blue dye purchased from Merck (Germany), distilled water, and N_2 gas.

2.2. Synthesis of Fe_3O_4

Fe_3O_4 was synthesized using the coprecipitation method. First, a total of 1.988 g $FeCl_2{\cdot}4H_2O$ and 5.406 g $FeCl_3{\cdot}6H_2O$ were dissolved in 20 mL of distilled water. Afterward, 1 M NaOH was added to the solution dropwise while slowly stirring with a magnetic stirrer at a speed of 100 rpm, and N_2 gas was emitted until the pH reached ± 10. The precipitate was separated from the solution using a magnet and washed several times with distilled water and ethanol until the pH was neutral. Finally, it was dried in an oven at 70ºC for 3 hours.

2.3. Synthesis of Fe_3O_4/SiO_2

The Fe_3O_4/SiO_2 was synthesized using the Stober method. First, 0.5 g Fe_3O_4 was dispersed in 20 mL of ethanol using an ultrasonic bath for 30 minutes at room temperature. The obtained product was added 5 mL of ammonia solution (28%), followed by the gradual addition of 2 mL TEOS solution (1 mL TEOS in 20 mL ethanol) using a magnetic stirrer for 3 for 5 hours. The precipitate was washed several times with distilled water and ethanol until the pH was neutral. The Fe_3O_4/SiO_2 were dried in an oven at a temperature of 70ºC for 3 hours.

2.4. Synthesis of Fe_3O_4/SiO_2/NiO

An amount of 0.5 g of $NiCl_2{\cdot}6H_2O$ was dispersed in 10 mL of DEG for 30 minutes at room temperature using a water bath sonicator, followed by adding 0.5 g of Fe_3O_4/SiO_2 and 10 mL of 0.0025 M NH_4HCO_3 solution under stirring for 15 minutes. The mixture was transferred to a Teflon autoclave and heated at 120 for 5 hours. The precipitate was washed using distilled water and ethanol. The obtained product was dried in an oven at 70ºC for 3 hours. Finally, it is calcined at a temperature of 300ºC for 2 hours.

2.5. Characterization

The product obtained was identified using an X-ray diffractometer (XRD Panalytical), operated at 40 kV and 30 mA, Cuα (λ = 1.542 Å) as a radiation source, and a range of 2θ at 10-90°. The bond formation was analyzed with Fourier Transform Infra-Red spectroscopy (FTIR, Prestige 21, Shimadzu) at wave numbers of 400-4000 cm^{-1} using the KBr pellet technique. Furthermore, the specific surface areas were evaluated with N_2 adsorption-desorption using the BET (Quantachrome QuadraWin) method. Scanning electron microscopy with an energy dispersive spectrometer (SEM-EDS JSM 6510) was used to observe surface morphology and elemental composition. Additionally, magnetic properties were evaluated using a Vibrating Sample Magnetometer (VSM Oxford Type 1.2 T). UV-Vis Diffuse Reflectance Spectroscopy (Pharmaspec, UV-1700) was used to determine the band gap at 200-800 nm wavelengths. The concentration of methylene blue dye was determined using a UV-Vis spectrophotometer (Type Orion Aquamate 8000).

2.6. Photocatalytic activity

Photocatalytic activity of Fe_3O_4/SiO_2/NiO against methylene blue dye under UV light irradiation source (15-W x 3, Philips). In the experiment, 50 mL methylene blue dye at a concentration of 20 mg/L with a 0.5 g/L catalyst dose, the pH of the solution was varied at 5, 6, 7, 8, 9, and 10 using 0.1 M HCl or NaOH. The mixture was stirred in a dark room for 40 minutes to reach equilibrium, followed by a photocatalytic degradation process for 120 minutes (20 minutes intervals). Other variables are catalyst dose (0.25, 0.5, 0.75 and 1.0 g/L) and the dye concentration (10, 20, 30, and 40 mg/L).

The reusability of the catalyst was assessed by magnetically separating it following photocatalytic degradation under optimal conditions. It was then washed using deionized water and dried in an oven for 3 hours at 70°C. Calcination was carried out at 300ºC for ± 2 hours to remove organic substances (Prasad *et al.,* 2022). Finally, the catalyst is reused for photocatalytic degradation and repeated up to 5 times.

3. Results and discussion

3.1. Catalyst characterization

Fe_3O_4 as the core was synthesized and coated SiO_2 using the coprecipitation and the sol-gel methods, respectively. The $Fe_3O_4/SiO_2/NiO$ was synthesized using the hydrothermal technique. Figure 1 shows that the crystal structure of Fe_3O_4, Fe_3O_4/SiO_2, and $Fe_3O_4/SiO_2/NiO$ were determined using XRD. According to the cubic spinel phase (JCPDS card no. 74-0748), the diffraction characteristics of Fe_3O_4 were observed at 2θ = 30.39°, 35.69°, 43.35°, 53.87°, 57.65°, and 62.97°. This was appropriate for the planes (220), (311), (400), (422), (511), and (440). After coating with SiO_2, a broad peak was observed at 2θ around 23°. This peak is a characteristic of amorphous SiO_2 (Chen *et al.,* 2014).

The new peaks in $Fe_3O_4/SiO_2/NiO$ were observed at 2θ = 76.01° (311) and 80.05° (222). Meanwhile, other peaks overlapped those of Fe_3O_4, including 37.21° (111), 43.45° (200), and 62.95° (220), according to the structure of JCPDS card no. 78-0423 (NiO). Using the Debye-Scherrer equation, the crystal size of Fe_3O_4 was calculated to be 7.0 nm, while those of Fe_3O_4/SiO_2 and $Fe_3O_4/SiO_2/NiO$ were 8.2 nm. Another research showed that coating Fe_3O_4 with SiO_2 increased the crystal size from 22.60 to 38.0 nm (Reman *et al.,* 2021).

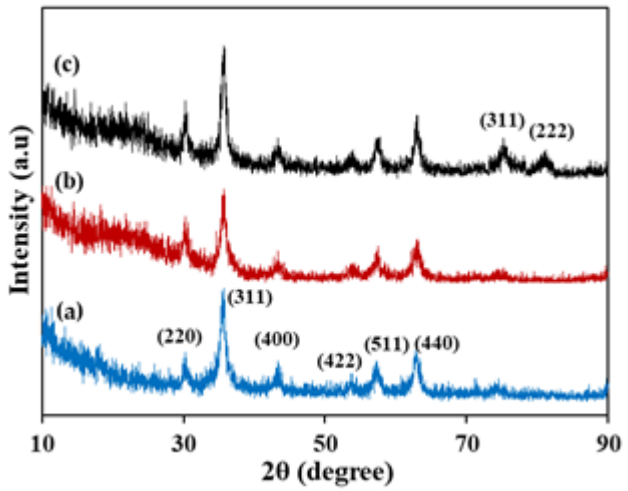

Figure 1. XRD diffraction pattern of (a) Fe_3O_4, (b) Fe_3O_4/SiO_2, and (c) $Fe_3O_4/SiO_2/NiO$

Figure 2 shows the FTIR spectra of Fe_3O_4, Fe_3O_4/SiO_2, and $Fe_3O4/SiO_2/NiO$. The wave numbers between 3400 cm^{-1} and 1600 cm^{-1} appear in all peaks, indicating the presence of O-H groups from free water, which is absorbed by the catalyst (Hariani *et al.,* 2021; Elzahrani 2017; Ojemaye *et al.,* 2017). In Figure 2(a), Fe-O stretching vibration is observed at a wave of 557.43 cm^{-1}. Meanwhile, no other peak was observed apart from water absorption. Figure 2b shows an additional peak at 464.84 and 804.31 cm^{-1}, which indicates symmetrical and asymmetrical Si-O terminals (Reman *et al.,* 2021). A strong peak at 1089.78 cm^{-1} is an asymmetric Si-O-Si and Si-O-H vibrational bond observed at a wave number of 950.60 cm^{-1} (Fu *et al.,* 2019; Han and An, 2021). The wave number for metal-oxygen stretching vibration was observed in the 400-700 cm^{-1} range. The absorption band in the 600–700 cm^{-1} indicates absorptions of Ni-O stretching vibration. This study appears at 670.32 cm^{-1}, even though it is not sharp (Qiao *et al.,* 2009).

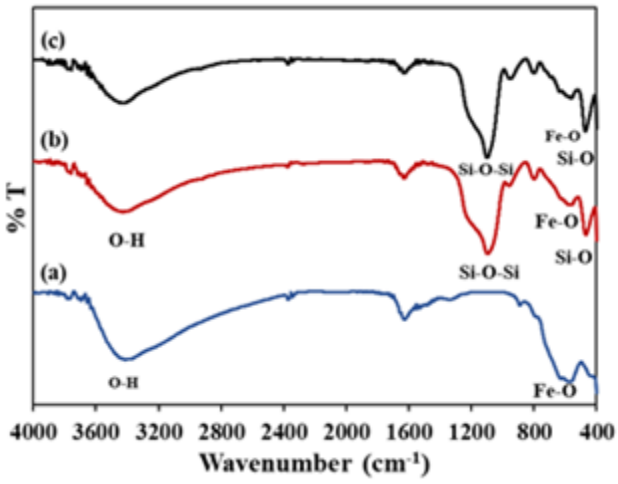

Figure 2. FTIR spectra of (a) Fe_3O_4, (b) Fe_3O_4/SiO_2, and (c) $Fe_3O_4/SiO_2/NiO$

The surface area affects the catalyst's ability in the degradation process (Kalam *et al.,* 2018). Based on the N_2 gas adsorption-desorption curve shown in Figure 3, the specific surface area (S_{BET}) of Fe_3O_4, Fe_3O_4/SiO_2, and $Fe_3O_4/SiO_2/NiO$ were determined using BET analysis. According to the classification IUPAC, all BET curves showed compliance with the Type IV isotherm, namely mesoporous materials. The specific surface area of Fe_3O_4 (S_{BET}) is 88.4 m^2/g, but after coating with SiO_2, it becomes 124.2 m^2/g. SiO_2 protects it from agglomeration processes, thereby increasing the surface area (Li *et al.,* 2017; Wu *et al.,* 2020). Another research showed that coating Fe_3O_4 with graphene oxide (GO) produces a larger surface area than Fe_3O_4 and GO (Thy *et al.,* 2020). In this study, the $Fe_3O_4/SiO_2/NiO$ has a larger surface area than Fe_3O_4 and Fe_3O_4/SiO_2, which are 128.8 m^2/g. These results are similar to $CoFe_2O_4/SiO_2/TiO_2$, which have a larger surface area than $CoFe_2O_4$ and $CoFe_2O_4/SiO_2$ (Zielińska-Jurek *et al.,* 2017).

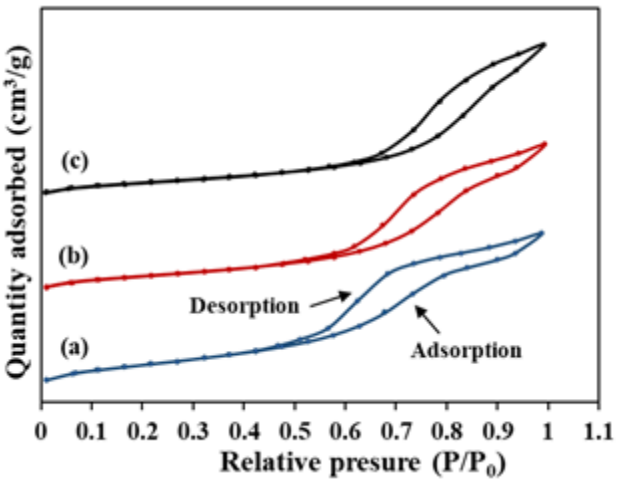

Figure 3. N_2 adsorption-desorption isotherm of (a) Fe_3O_4, (b) Fe_3O_4/SiO_2, and (c) $Fe_3O_4/SiO_2/NiO$

Figure 4 presents the morphology of Fe_3O_4, Fe_3O_4/SiO_2, and $Fe_3O_4/SiO_2/NiO$ analyzed using SEM. The Fe_3O_4 surface appears to be small, dense, and agglomerated, while the Fe_3O_4/SiO_2 and $Fe_3O_4/SiO_2/NiO$ appear to be a granular molecule with reasonably large sizes coating Fe_3O_4. The SEM mapping of the $Fe_3O_4/SiO_2/NiO$ in Figure 5 shows the distribution of elements on the composite surface. Some parts of the surface indicate the agglomeration of Fe_3O_4 (red). Meanwhile, Ni (blue) appears to be distributed on the surface of Fe_3O_4/SiO_2 and Fe_3O_4.

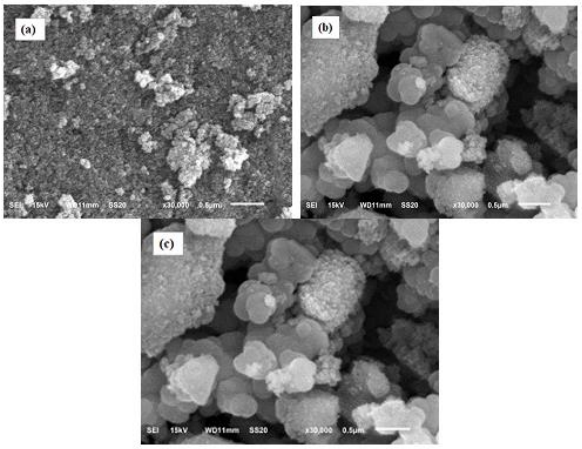

Figure 4. Morphology of (a) Fe_3O_4, (b) Fe_3O_4/SiO_2, and (c) $Fe_3O_4/SiO_2/NiO$

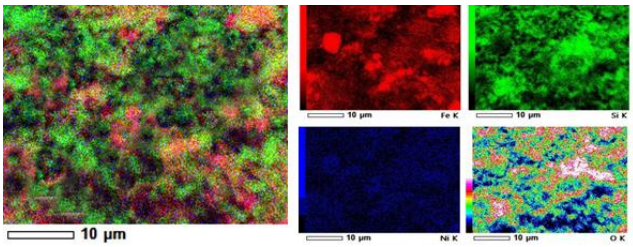

Figure 5. SEM Maping of $Fe_3O_4/SiO_2/NiO$

Table 1 shows the composition of Fe_3O_4, Fe_3O_4/SiO_2, and $Fe_3O_4/SiO_2/NiO$ as a result of EDX analysis. The composition of Fe_3O_4 consists of Fe and O, which indicates its purity. The addition of Si to Fe_3O_4/SiO_2 indicates that SiO_2 has successfully to coating Fe_3O_4, while the addition of Ni shows that the element was distributed on the surface of Fe_3O_4/SiO_2.

Figure 6 shows the magnetic properties of Fe_3O_4, Fe_3O_4/SiO_2, and $Fe_3O_4/SiO_2/NiO$. The Fe_3O_4 saturation magnetization of 83.26 emu/g is classified as strong magnetization. Previous research showed that nanomagnetic coating ferrite with non-magnetic materials reduces saturation magnetization. Subsequently, coating Fe_3O_4 with SiO_2 blocks the interaction of the magnetic dipole between adjacent magnetic particles and isolates them from the magnetic field (Kotutha *et al.,* 2019). In general, SiO_2 is non-magnetic, which implies that it is insulating and inert. In this research, the saturation magnetization values of Fe_3O_4/SiO_2 and $Fe_3O_4/SiO_2/NiO$ were 61.96 and 53.84 emu/g, respectively. The presence of NiO reduces the properties of Fe_3O_4/SiO_2. This is related to the surface effect and anisotropy of the particles (Zhao *et al.,* 2015; Sadeghi *et al.,* 2012). The magnetization curve shows a mixture of ferromagnetic and superparamagnetic properties. Therefore, the magnetic properties allow for the easy separation of the composite from the solution after being used for photocatalytic degradation.

The energy absorbed by the catalyst depends on the optical band gap energy, namely the difference between the valence and conduction bands (Kalam *et al.,* 2018). Figure 7 shows plots $(\alpha hv)^2$ versus Energy (eV) to obtain band gap values of $Fe_3O_4/SiO_2/NiO$. The broad spectrum indicates that Fe_3O_4 dominates the phase in the material. Finally, the band gap value is obtained from Tauc's plot according to the following equation.

$$(\alpha h\nu)^2 = A(h\nu - E_g) \quad (1)$$

Where α, A, h, ν, and E_g are the absorption coeffi-cient, proportionality constant, Planck's constant, vibra-tional frequency, and energy band gap. NiO was absorbed in a wavelength of 320 nm. Another research showed that NiO and Fe_3O_4 were observed at 330 nm and 440 nm, respectively (Barzinjy *et al.,* 2020). In this research, the $Fe_3O_4/SiO_2/NiO$ band gap was 2.83 eV, which is smaller than the band gap of NiO ~ 3.5 eV and larger than the band gap of ferrite compounds ~ 2 eV (Hariani *et al.,* 2021). The formation of the core-shell-shell, namely the $Fe_3O_4/SiO_2/NiO$, successfully reduced the band gap.

3.2. Photocatalytic activity

Figure 8a shows the effect of pH on the efficiency of photocatalytic degradation. The dye concentration was 20 mg/L, and the catalyst dose was 0.5 g/L with a pH varying from 5 to 10. The pH solution contributes to the degradation of dyestuffs and gives a charge to the catalyst's surface. Photocatalytic degradation of methylene blue dye using several catalysts, namely TiO_2, ZnO, Co_3O_4, CdS, and $MnTiO_3$, was optimum at a pH range of 9 to 11 (Alkaykh *et al.,* 2020; Alkaim *et al.,* 2014). Methylene blue dye is a cationic dye at alkaline pH, the dye has a positive charge, and the interaction is more effective with a negatively charged catalyst. Furthermore, there are many OH^- ions at the pH of alkaline solutions. The catalyst absorbs irradiation to produce holes (h_{VB}^+) which then react with OH^- to form hydroxyl radicals (•OH). At high pH, hydroxyl radicals are quickly scavenged, giving them no opportunity to react with dyes (Alkaim *et al.,* 2014).

Table 1. EDX analysis of Fe_3O_4, Fe_3O_4/SiO_2, and $Fe_3O_4/SiO_2/NiO$

Materials	Elements (%)			
	O	Fe	Si	Ni
Fe_3O_4	29.70	70.30	-	-
Fe_3O_4/SiO_2	53.51	18.60	27.89	-
$Fe_3O_4/SiO_2/NiO$	53.28	14.64	23.97	8.11

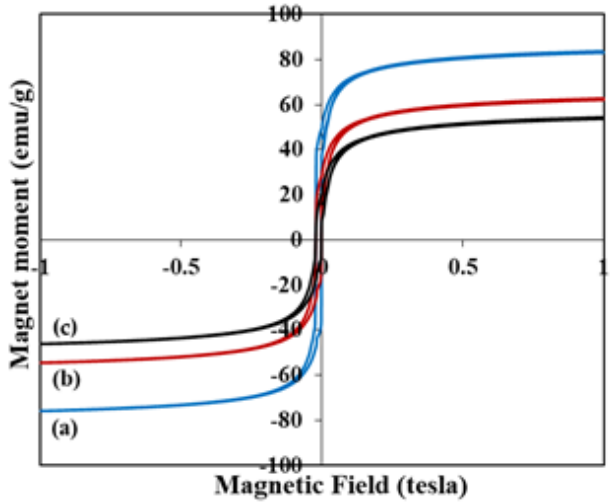

Figure 6. The magnetization of (a) Fe_3O_4, (b) Fe_3O_4/SiO_2 and (c) $Fe_3O_4/SiO_2/NiO$

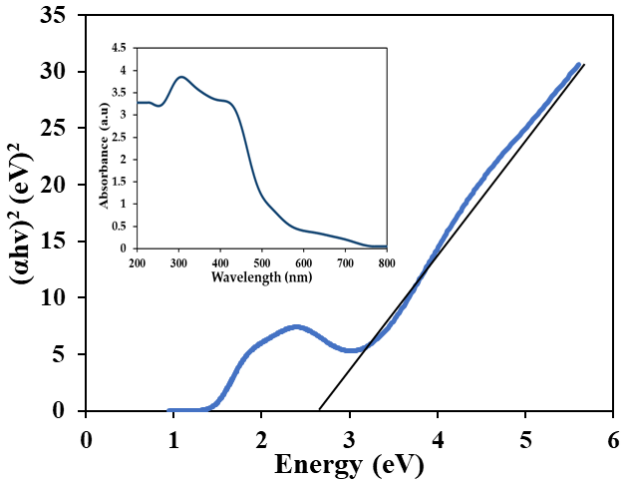

Figure 7. Wood-Tauc plot for $Fe_3O_4/SiO_2/NiO$

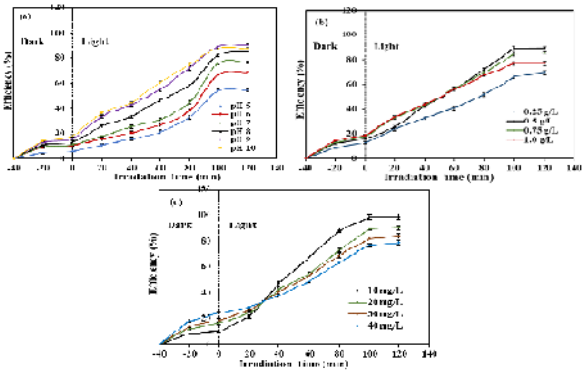

Figure 8. Effect of (a) pH solution, (b) catalyst dose, and (c) initial concentration of dye on the photocatalytic degradation of the $Fe_3O_4/SiO_2/NiO$

The effect of catalyst doses was conducted with variations of 0.25, 0.5, 0.75, and 1.0 g/L, while the concentration was 20 mg/L at a pH of 9. Figure 8b shows that the higher the amount of catalyst, the more the dye degraded. In addition to being observed at 100 minutes, doses of 0.5 and 0.75 g/L had nearly the same degradation rate. However, there was a decrease at 1.0 g/L. At higher doses, there is a reduction in the reaction rate due to catalyst loading, which causes the deactivation of activated molecules by collision with ground state catalysts (Herman, 1995). Furthermore, the optimum dose was at 0.5 g/L with a dye reduction efficiency of 89.77% in 100 minutes.

The effect of the initial dye concentration was analyzed using 10 to 50 mg/L. Figure 8c shows that the dye reduction efficiency increased directly with the initial dye concentration after 100 min. It also increases with the number of dye molecules adsorbed on the catalyst surface. This prevents photons from reaching the catalyst surface as they are blocked by the dye (Hariani *et al.,* 2022; Makeswari and Saraswathi, 2020). Therefore, the photocatalytic degradation of methylene blue dye was better at a low concentration of 10 mg/L with an efficiency of 98.51%. This indicates that the catalyst plays a significant role in dye degradation.

The mechanism of photocatalytic degradation of methylene blue (MB) dye using $Fe_3O_4/SiO_2/NiO$ composite according to the reaction: (Ammar *et al.*, 2020).

$Fe_3O_4/SiO_2/NiO + h\nu \rightarrow Fe_3O_4/SiO_2/NiO\ (e_{CB}^- + h_{VB}^+)$

$e_{CB}^- + O_2 \rightarrow \cdot O_2^-$

$h_{VB}^+ + H_2O \rightarrow \cdot OH + H^+$

$\cdot O_2^- + H^+ \rightarrow \cdot OH_2$

$\cdot O_2^- + H_2O \rightarrow \cdot HO_2 + OH^-$

$\cdot OH_2 + H_2O \rightarrow H_2O_2 + \cdot OH$

$H_2O_2 \rightarrow 2\cdot OH$

$MB\text{-}Fe_3O_4/SiO_2/NiO + \cdot OH + \cdot O_2^- \rightarrow Fe_3O_4/SiO_2/NiO + CO_2 + H_2O + \text{other product}$

3.3. Kinetic for photodegradation

The following formula expresses the kinetic model of photocatalytic degradation on methylene blue dye using pseudo-first-order:

$$\ln C_0 / C_t = kt \qquad (2)$$

Where C_0 and C_t are the initial concentration at each time (a certain time) (mg/L), t is the irradiation time (min), and k is the rate constant (min^{-1}). The k value is obtained from the slope of the linear fitting graph ln C_0/C_t Versus t. This research determined the kinetics of photocatalytic degradation using a methylene blue dye concentration of 10 mg/L, a catalyst dose of 0.5 g/L, and a solution pH of 9 (Figure 9). The coefficient of determination value (R^2= 0.990 > 0.9) indicates that the kinetic model is compatible (Van *et al.*, 2019). Therefore, the k value obtained is $1.1.10^{-4}$ min^{-1}.

3.4. Reusability of $Fe_3O_4/SiO_2/NiO$

Reusability is essential for the remediation process as it aims to see the cost-effectiveness and feasibility of catalysts (Gebrezgiabher *et al.,* 2019; Moosavi *et al.,* 2020). Its performance uses methylene blue dye

concentration of 10 mg/L, a dose of 0.5 g/L, and a solution of pH 9. Figure 10 shows the efficiency of photocatalytic degradation after 5 cycles. Subsequently, the efficiency of photocatalytic degradation decreased from 98.02 to 94.97% (< 5%). The photocatalyst properties, such as surface area, number of active sites, and the presence of impurities, could change during reuse, but those with approximately 5 cycles continue to show good performance. It can be believed that the Fe_3O_4/SiO_2/NiO exhibits excellent photocatalyst stability.

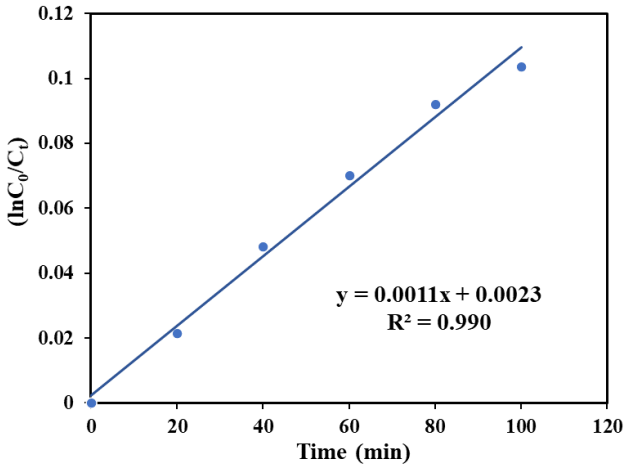

Figure 9. The plot of the pseudo-first-order for photocatalytic degradation on methylene blue dye

Table 2 shows a degradation efficiency comparison of methylene blue dye using several catalysts. The results of this research have high degradation efficiency with the same initial concentration and relatively fast time.

The core-shell-shell composite Fe_3O_4/SiO_2/NiO has been successfully synthesized, with Fe_3O_4 as the core, SiO_2 as the interlayer, and NiO spread on the composite surface. The composite has magnetic properties with a saturation magnetization value of 53.84 emu/g. Furthermore, the optimum conditions for photocatalytic degradation of Fe_3O_4/SiO_2/NiO against methylene blue dye were pH 9, catalyst dose of 0.5 g/L, 10 mg/L dye concentration, and irradiation time of 100 minutes, the degradation efficiency of 98.51%. This composite has high stability, and reusability of approximately 5 cycles decreases the removal efficiency by < 5%. Therefore, the Fe_3O_4/SiO_2/NiO composite has the potential to reduce water pollution. Further research needs to be developed for the photocatalytic degradation of wastewater containing other pollutants.

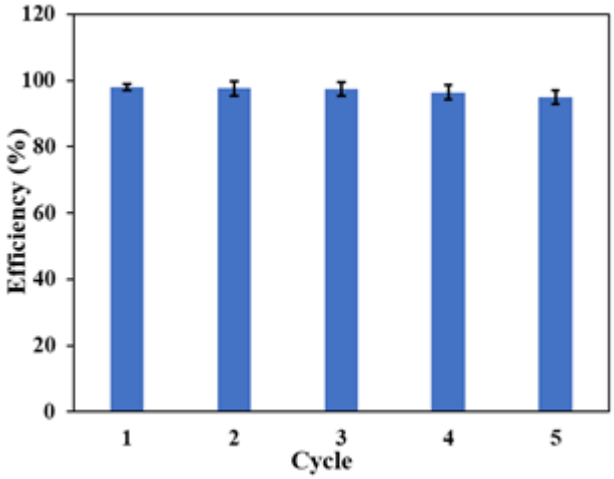

Figure 10. Reusability of Fe_3O_4/SiO_2/NiO

4. Conclusion

Table 2. Photocatalytic degradation efficiency of some catalysts againts methylene blue dye

Catalyst	Initial concentration (mg/L)	Irradiation time (min)	Efficiency(%)	References
Cu-TiO_2/ZnO	35	120	64.72	Khaki *et al*. (2017)
SnS_2-SiO_2@α-Fe_2O_3	5	100	96.0	Balu et al. (2018)
ZnO-SnO_2	10	60	96.53	Lin et al. (2018)
TiO_2/Alg/FeNPs	5	120	97.6	Kanakaraju *et al.* (2018)
$CoFe_2O_4/H_2O_2$	10	140	82.0	Kalam *et al*. (2018)
Fe_3O_4@SiO_2@CeO_2	10	50	98.0	Ziaadini *et al*. (2019)
$CoFe_2O_4$@SiO_2@$DyCe_2O_7$	20	30	94.5	Zinatloo-Ajabshir and Salavati-Niasari (2019)
Fe_2TiO_5	10	250	97.0	Vasiljevic *et al*. (2020)
Fe_3O_4/SiO_2/NiO	10	100	98.51	Present study

Acknowledgements

This research was funded by the Ministry of Education, Culture, Research and Technology for providing funding assistance through the *Penelitian Dasar Unggulan Perguruan Tinggi* (PDUPT) in 2022 as additional research output. Contract No. 0063.01/UN9.3.1/PL/2022.

References

Ali M., Sarkar A., Pandey M.D., and Pandey S. (2006). Efficient precipitation of dyes from dilute aqueous solutions of ionic liquids. *Analytical sciences*, **22**, 1051–1053.

Alkaim A.F., Aljeboree A.M., Alrazaq N.A., Baqir S.J., Hussein F.H., and Lili A.J. (2014). Effect of pH on adsorption and photocatalytic degradation efficiency of different catalyst on removal of Methylene blue, *Asian Journal of Chemistry*, **26**, 8445–8448.

Alkaykh S., Mbarek A. and Ali-Shattle E.E. (2020). Photocatalytic degradation of methylene blue dye in aqueous solution by $MnTiO_3$ nanoparticles under sunlight irradiation, *Heliyon*, 6, 1–6.

Ammar S.H., Elaibi A.I., and Mohamme I.S. (2020). Core/shell Fe_3O_4@Al_2O_3-PMo magnetic nanocatalyst for photocatalytic

degradation of organic pollutants in an internal loop airlift reactor, *Journal of Water Process Engineering*, **37**, 1–11

Balu S, Uma K., Pan G.T., Yang T.C. and Ramaraj S.K. (2018). Degradation of methylene blue dye in the presence of visible light using SiO_2@α-Fe_2O_3 nanocomposites deposited on SnS_2 flowers, *Materials*, **6**, 1030.

Barakat A., Al-Noaimi M., Suleiman M. *et al.* (2013). One Step Synthesis of NiO Nanoparticles via Solid-State Thermal Decomposition at Low-Temperature of Novel Aqua (2,9-dimethyl-1,10-phenanthroline) $NiCl_2$ Complex, *International Journal of Molecular Sciences*, **14**, 23941–23954.

Barzinjy A.A., Hamad S.M., Aydin S., Ahmed M.H., and Hussain F.H.S. (2020). Green and eco-friendly synthesis of Nickel oxide nanoparticles and its photocatalytic activity for Methyl orange degradation, *Journal of Materials Science: Materials in Electronics*, **31**, 11303–11316.

Behzadi S., Nonahal B., Royaee S.J., and Asadi A.A. (2020). TiO_2/SiO_2/Fe_3O_4 magnetic nanoparticles synthesis and application in Methyl orange UV photocatalytic removal, *Water Science and Technology*, **11**, 2432–2445.

Channei D., Inceesungvorn B., Wetchakun N., and Phanichphant S. (2014). Synthesis of Fe_3O_4/SiO_2/CeO_2 core–shell magnetic and their application as photocatalyst, *Journal of Nanoscience and Nanotechnology*, **14**, 7756–7762.

Chen F., Yan F., Chen Q., Wang Y., Han L., Chen Z., and Fang S. (2014). Fabrication of Fe_3O_4@SiO_2@TiO_2 nanoparticles supported by graphene oxide sheets for the repeated adsorption and photocatalytic degradation of rhodamine B under UV irradiation, *Dalton Transactions*, **43**, 13537–13544.

Chen X., Wu Z., Liu D., and Gao. (2017). Preparation ZnO photo-catalyst for the efficient and rapid photocatalytic degra-dations of azo dyes, *Nanoscale Research Letters*, **12**, 143.

David P.S., Karananithi A. and Fathima N.N. (2020). Improved filtration for dye removal using keratin-polymide blend nanofibrous membranes, *Environmental Science and Pollution Research*, **27**, 45629–45638.

Dias N.C., Bassin J.P., and Sant'Anna G.L. (2019). Ozonation of the dye reactive red 239 and biodegradation of ozonation products in a moving-bed biofilm reactor: revealing reaction products and degradations pathways, *International Biodeterioration & Biodegradation*, **144**, 1–9.

D'Amario L., Fohlinger J., Boschloo G., and Hammarstrom L. (2018). Unveiling hole trapping and surface dynamics of NiO nanoparticles, *Chemical Science*, **9**, 223–230.

Elzahrani E. (2017). Photodegradation of binary azo dyes using core-shell Fe_3O_4/SiO_2/TiO_2 nanospheres, *American Journal of Analytical Chemistry*, **8**, 95–115.

Fu C., Liu X., Wang Y., Li L., and Zhang Z. (2019). Preparation and characterization of Fe_3O_4@SiO_2@TiO_2-Co/rGO magnetic visible light photocatalyst for water treatment, *RSC Advances*, **9**, 20256–20265.

Gao P., Liu J., Sun D.D., and Ng W. (2013). Graphene oxide-CdS composite with high photocatalytic degradation and disinfection activities under visible light irradiation, *Journal of Hazardous Materials*, **250**, 412–2420.

Gebrezgiabher M., Gebreslassie G., Gebretsadik T., Yeabyo G., Elemo F., Bayeh Y., Thomas M. and Linert W. (2019). AC-Doped TiO_2/Fe_3O_4 nanocomposite for photocatalytic dye degradation under natural sunlight irradiation, *Journal of Composites Science*, **3**, 75.

Girginova P.I., Daniel-da-Silva A.L., Lopes C.B., Figueira P., Otero M., Amaral V.S., Pereira E., and Trindade T. (2010). Silica coated magnetite particles for magnetic removal of Hg^{2+} from water, *Journal of Colloid and Interface Science*, **345**, 234–240.

Han J.S., and An G.S. (2021). Preparation of Dual-Layered Core–Shell Fe_3O_4@SiO_2 nanoparticles and their properties of plasmid DNA purification, *Nanomaterials*, **11**, 3422.

Hariani P.L., Said M., Rachmat A., Riyanti F., Pratiwi H.C., and Rizki W.T. (2021). Preparation of $NiFe_2O_4$ nanoparticles by solution combustion method as photocatalyst of congo red, *Bulletin of Chemical Reaction Engineering & Catalysis*, **16**, 481–490.

Hariani P.L., Said M., Salni, Aprianti N. and Naibaho Y.A.L.R. (2022). High efficient photocatalytic degradation of methyl orange dye in an aqueous solution by $CoFe_2O_4$-SiO_2-TiO_2 magnetic catalyst, *Journal of Ecological Engineering*, **23**, 118–128.

Herman J.M. (1995). Heterogeneous photocatalysis; an emerging discipline involving multiphase system, *Catalyst Today*, **24**, 157–164.

Hosny N.M. (2011). Synthesis, characterization and optical band gap of NiO nanoparticles derived from anthranilic acid and precursors via a thermal decomposition route, *Polyhedron*, **30**, 470–476.

Hou C., Hu B., and Zhu J. (2018). Photocatalytic degradation of methylene blue over TiO_2 Pretreated with varying concentrations of NaOH, *Catalysts*, **8**, 575.

Jarariya R. (2022). A review based on spinel ferrite nanomaterials $MgFe_2O_4$ - synthesis of photocatalytic dye degradation in visible light response, *Journal of Environmental Treatment Techniques*, **10**, 149–2156.

Kanakaraju D., Shahdad N.R.M., Lim Y., and Pace. A. (2018). Magnetic hybrid TiO_2/Alg/FeNPS triads for the efficient removal of Methylene blue from water, *Sustainable Chemistry and Pharmacy*, **8**, 50–62.

Kalam A., Al-Sehemi A.G., Assiri M. *et al.* (2018), Modified solvothermal synthesis of cobalt ferrite ($CoFe_2O_4$) magnetic nanoparticles photocatalysts for degradation of Methylene blue with H_2O_2/visible light, *Results in Physics*, **8**, 1046–1053.

Khaki M.R.D., Shafeeyan M.S., Raman A.A.A. and Daud W.M.A.W. (2017), Evaluating the efficiency of nano-sized Cu doped TiO_2/ZnO photocatalyst under visible light irradiation, *Journal of Molecular Liquids*, **258**, 354–365.

Khan N.A., Saeed K., Khan I. *et al.* (2022). Efficient photodegradation of orange II dye by nickel oxide nanoparticles and nanoclay supported nickel oxide nanocomposite, *Applied Water Science*, **12**, 1–10.

Khodai M., Ghasemi N., Moradi B., and Rahimi M. (2013). Removal of methylene blue from wastewater by adsorption onto $ZnCl_2$ activated corn husk carbon equilibrium studies, *Journal of Chemistry*, **3**, 1–7.

Kotutha I., Duangchuen T., Swatsitang K., Meewasana W., Khajonrit J., and Maensiri S. (2019). Electrochemical properties of rGO/$CoFe_2O_4$ nanocomposites for energy storage application, *Ionics*, **25**, 5401–5409.

Kuang Y., Zhang X., and Zhou S. (2020). Adsorption of methylene blue in water onto activated carbon by surfactant modification, *Water*, **12**, 587.

Lett J.A., Sagadevan S., Weldegebrieal G.K., and Fatimah I. (2022). Hydrothermal synthesis and photocatalytic activity of

NiO nanoparticles under visible light illumination, *Bulletin of Chemical Reaction Engineering & Catalysis*, **17**, 2, 340–349.

Lin J., Luo Z., Liu J., and Li P. (2018). Photocatalitic degradation of methylene blue in aqueous solution by using ZnO-SnO_2 nanocomposites, *Materials Science in Semiconductor Processing*, **87**, 24–31.

Li Q., Lu C., Chen C., Xie L., Liu Y., Li Y., Kong Q., and Wang H. (2017). Layered $NiCo_2O_4$/ reduced graphene oxide composite as an advanced electrode for supercapacitor, *Energy Storage Materials*, **8**, 59–67.

Loan N.T.T, Hien Lan N.T.H, Hang N.T.T. *et al.* (2019). $CoFe_2O_4$ nanomaterials: effect of annealing temperature on characterization, magnetic, photocatalytic, and photo-Fenton properties, *Processes*, **7**, 885.

Makeswari M. and Saraswathi P. (2020). Photocatalytic degradation of methylene blue and methyl orange from aqueous solution using solar light onto chitosan bi-metal oxide composite, *SN Applied Sciences*, **2**, 336.

Moghaddam S.S., Moghaddam M.R.A. and Arami M. (2010). Coagulation/flocculation process for dye removal using sludge from water treatment plant: optimization through response surface methodology, *Journal of Hazardous Materials*, **175**, 651–657.

Moosavi S., Li R.Y.M., Lai C.W. *et al.* (2020). Methylene blue dye photocatalytic degradation over synthesized Fe_3O_4/AC/TiO_2 nano-catalyst: degradation and reusability studies, *Nanomaterials*, **10**, 2360.

Ojemaye M.O., Okoh O.O., and Okoh A.I. (2017). Performance of $NiFe_2O_4$-SiO_2-TiO_2 photocatalyst for the effective photocatalytic re-duction of Cr(VI) from aqueous solutions, *Journal of Nanomaterials*, **2017**, 1–18.

Pham T.D., Bui T.T., Nguyen V.T. *et al.* (2018). Adsorption of polyelectrolyte onto nanosilica synthesized from rice husk: characteristics, mechanisms, and application for antibiotic removal, *Polymers*, **10**, 220.

Prasad K.S., and Shamshuddin S.Z.M. (2022). Highly efficient conversion of glycerol and t-butanol to biofuel additives over AlPO solid acid catalyst under microwave irradiation technique: kinetic study, *Comptes Rendus Chimie*, **25**, 149–170.

Qiao H., Wei Z., Yang H., Zhu L., and Yan X. (2009). Preparation and characterization of NiO nanoparticles by anodic arc plasma method, *Journal of Nanomaterials*, **2009**, 1–5.

Reman G U., Tahir M., Goh P.S., Ismail A.F., Hafeez A., and Khan I.U. (2021). Enhancing the photodegradation of phenol using Fe_3O_4/SiO_2 binary nanocomposite mediated by silane agent, *Journal of Physics and Chemistry of Solids*, **153**, 110022.

Sadeghi S., Azhdari H., Arabi H., and Moghaddam A.Z. (2012). Surface modified magnetic Fe_3O_4 nanoparticles as a selective sorbent for solid phase extraction of uranyl ions from water sampels, *Journal of Hazardous Materials*, **215**, 208–216.

Salomon R.V., Lydia I.S., Merlin J.P., and Venuvalingam P. (2012). Enhanced photocatalytic degradation of azo dye using nano Fe_3O_4, *Journal of the Iranian Chemical Society*, **9**, 101–109.

Thy L.T.M., Cuong P.M., Tu T.H., Nam H.M., Hieu N.H., and Phong M.T. (2020). Fabrication of magnetic iron oxide/graphene oxide nanocomposite for removal of lead ions from water, *Chemical Engineering Transactions*, **78**, 277–282.

Vandevivere P.C., Bianchi R., and Verstraete W. (1998). Treatment and reuse of wastewater from textile wet-processing industry: review of emerging technologies, *Journal of Chemical Technology and Biotechnology*, **72**, 289–302.

Van Tran T., Nguyen D.T.C., Le H.T.N. *et al.* (2019). A hollow mesoporous carbon from metal-organic framework for robust adsorbability of ibuprofen drug in water, *Royal Society Open Science*, **6**, 190058.

Vasiljevic Z.Z., Dojcinovic M.P., Vujancevic J.D. *et al.* (2020). Photocatalytic degradation methylene blue, under natural sunlight using iron titanate nanoparticles prepared by a modified sol-gel method, *Royal Society Open Science*, **7**, 1–15.

Wan X., Yuan M., Tie S., and Lan S. (2013). Effect of catalyst characters on photocatalytic activity and process of NiO nanoparticles in the degradation of methylene blue, *Applied Surface Science*, **277**, 40-46.

Wu Y., Shu R., Shan X., Zhang J., Shi J., Liu Y., and Zheng M. (2020). Facile design of cubic- like cerium oxide nanoparticles decorated reduced graphene oxide with enhanced microwave absorption properties, *Journal of Alloys and Compounds*, **817**, 152766.

Zhao P., Mo Z., Zhang P., Zhu X., and Guo R. (2015). Synthesis of graphene/Fe_3O_4/NiO magnetic nanocomposites and its application in photocatalytic degradation the organic pollutants in wastewater, *Journal of Porous Materials*, **22**, 1245–1253.

Ziaadini F., Mostafavia A., Shamspura T., and Fathirad F. (2019). Photocatalytic degradation of Methylene blue from aqueous solution using Fe_3O_4@SiO_2@CeO_2 core-shell magnetic nanostructure as an effective catalyst, *Advances in Environmental Technology*, **2**, 127–132.

Zielińska-Jurek A., Bielan Z., Dudziak S. *et al.* (2017), Design and application of magnetic photocatalysts for water treatment. The effect of particle charge on surface functionality, *Catalysts*, **7**, 360.

Zinatloo-Ajabshir S., and Salavati-Niasari M. (2019). Preparation of magnetically retrievable $CoFe_2O_4$@SiO_2@$Dy_2Ce_2O_7$ nanocomposites as novel photocatalyst for highly efficient degradation of organic contaminants. *Composites Part B: Engineering*, **174**, 106930.